Regional Characteristics of Attribution Risk on the Record-High-Temperature Event of 2022 Rainy Season in Japan

Rui Ito, Yukiko Imada, and Hiroaki Kawase

The attribution of 2022's high temperatures in Japan to human-induced climate change exhibits significant regional variability, with FARs of 0.33–1, influenced by large-scale wind changes and regional topography.

In early summer (late June–early July) of 2022, the rainy season in Japan was interrupted by an unseasonably enhanced anticyclone, resulting in record-high temperatures. The main island experienced unprecedented high temperatures in excess of those expected from the usual increase due to La Niña that year. In particular, the Tokyo metropolitan region recorded maximum temperatures over 10°C higher than usual, with temperatures exceeding 35°C lasting for nine days. The two-tier anticyclones that typically bring high temperatures to Japan (Imada et al. 2019; Shimpo et al. 2019; Inoue et al. 2021; Ito et al. 2022) resulted in the second-highest temperature at 850 hPa since 1960 (online supplemental 1; https://doi.org/10.1175/BAMS-D-23-0172.2).

The impact of human-induced climate change on several previous high-temperature events in Japan has been reported (e.g., Takahashi et al. 2016; Imada et al. 2019). The 2022 high-temperature event was also influenced by human-induced change, and the fraction of attributable risk (FAR; Allen 2003) estimated from averaged 850-hPa temperatures over Japan was exceeded 0.998 (online supplemental 1). However,

AFFILIATIONS: **Ito**—Japan Agency for Marine-Earth Science and Technology, Yokohama, and Meteorological Research Institute, Japan Meteorological Agency, Tsukuba, Japan; **Imada**—Atmosphere and Ocean Research Institute, The University of Tokyo, Kashiwa, Japan; **Kawase**—Meteorological Research Institute, Japan Meteorological Agency, Tsukuba, Japan

https://doi.org/10.1175/BAMS-D-23-0172.1

CORRESPONDING AUTHOR: Rui Ito, rui.ito@jamstec.go.jp

Publisher's Note: A modification was made to this article on 1 December 2023. In the section labeled "Large-ensemble dataset with GCM and RCM", the 5-km RCM simulations of the normal climate were initialized on every 24 July from 1980 to 2010, not from 1981 as initially published.

Supplemental material: https://doi.org/10.1175/BAMS-D-23-0172.2

In final form 29 September 2023

on a regional scale, variations in the impacts are possible. Particularly, various regional climatological characteristics result from the complex mountainous topography, which raises surface air temperatures sharply in leeward areas, such as the foehn effect.

Therefore, to investigate the potential impacts of human-induced climate change on regional-scale high-temperature events, we utilize large-ensemble downscaling simulations from atmospheric global circulation model (GCM) output using a regional climate model (RCM). The highest available resolution of our RCM is 5 km, enabling representation of the complicated topography of Japan (Fig. 1a).

Large-ensemble dataset with GCM and RCM

We used the atmospheric GCM (Mizuta et al. 2012) and the nonhydrostatic RCM (Sasaki et al. 2008) developed by the Meteorological Research Institute, Japan Meteorological Agency (JMA). Two domains covering all of Japan were set for the RCM downscaling simulations and a two-step one-way nesting strategy was applied, wherein the RCM simulations at 5 km were driven by those at 20 km, which were in turn driven by the GCM simulations at approximately 60 km.

We conducted two kinds of large-ensemble downscaling simulations. The first, HIST2022 is a factual simulation to represent the 2022 early summer with 100-ensemble members; observed sea surface temperatures (SST) and sea ice (SIC) from COBE-SST2 (Hirahara et al. 2014) were prescribed, together with all historical external forcings including greenhouse gases,

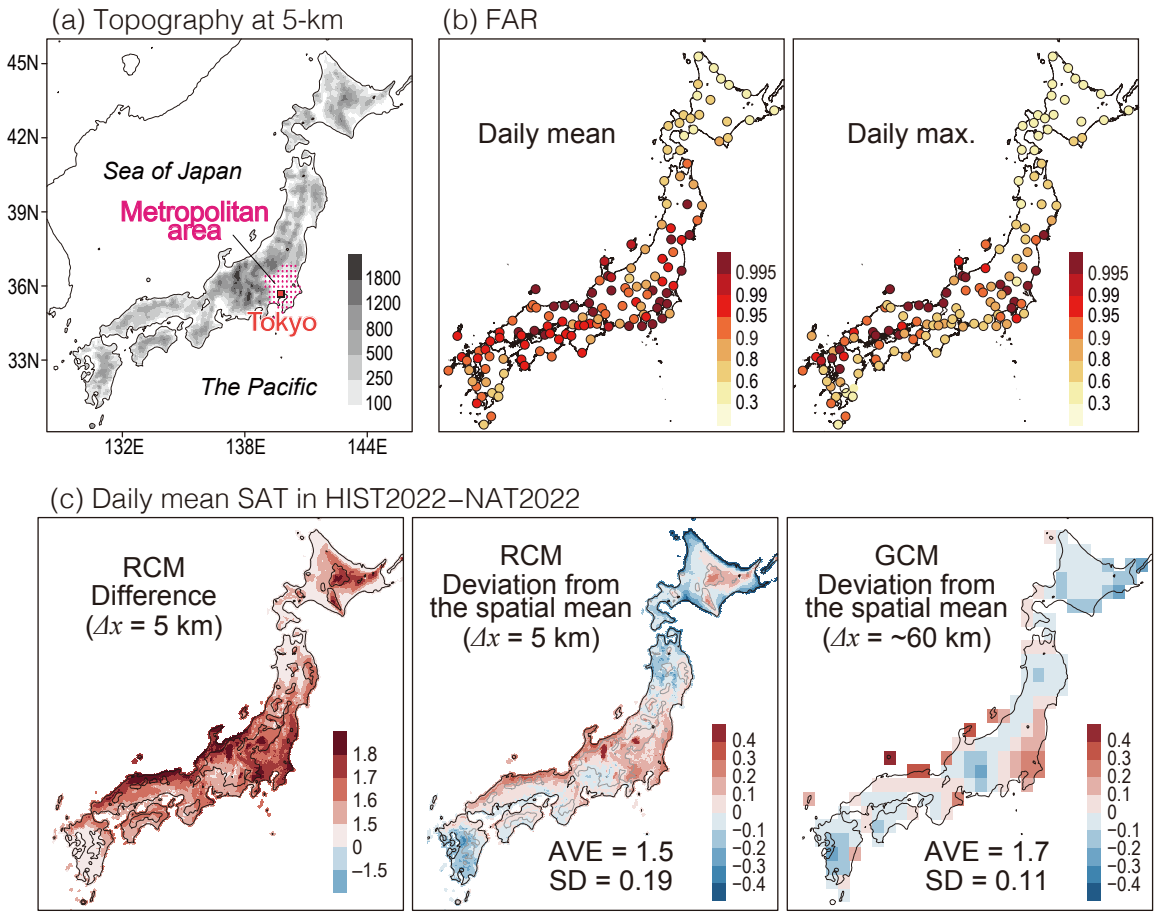

Fig. 1. (a) Topography (m) represented by the RCM at a grid spacing of 5 km. (b) FAR estimated from daily mean and daily maximum SATs. (c) Difference of daily mean SAT (HIST2022—NAT2022; °C). (left) Differences in the RCM and (center),(right) deviation from the spatially averaged difference over the land of Japan in the RCM and GCM, respectively. Gray contours over land represent an altitude of 600 m.

ozone, and aerosols. The second, NAT2022, is a counterfactual simulation with natural forcings set to the 1850 level. As a reference, 12-member-ensemble year-round simulations for the normal climate from 1981 to 2010 (HISTc and NATc, respectively) were also used, which are part of a database for policy decision-making for future climate change (d4PDF; Mizuta et al. 2017). The initial and lower boundary conditions were perturbed to create their ensembles. The 5-km RCM simulations for the 2022 event ran from 29 May 2022 and those for the normal climate using a time-slice approach were initialized on every 24 July from 1980 to 2010. We analyzed 8 days from 25 June to 2 July, the period of consecutively high temperatures. Here, the HIST2022 and NAT2022 simulations in July were driven by the SST and SIC data from the JMA seasonal forecasts initialized on 1 July, as COBE-SST2 data were unavailable when we conducted the experiments. The impact on results was negligible. For more on the model settings and model skills, see Mizuta et al. (2017) and Imada et al. (2017) for the GCM simulations, and Kawase et al. (2023) for the RCM simulations.

The FAR was calculated from the probabilities of exceeding the 2022 high temperature at ground observation sites. The simulated surface air temperature (SAT) was bias corrected using the method in Piani et al. (2010). Probability density functions were obtained using the kernel smoothing method (Marshall and Molteni 1993). The bias-corrected daily mean (maximum) SAT improved the climatological mean by 0.18°C (0.21°C) in the spatial mean bias and 0.18°C (0.21°C) in the root mean square error.

Impacts of human-induced climate change on surface air temperatures

Figure 1b illustrates the FAR calculated using SATs derived from the 2022 simulations with the 5-km RCM. Spatial variation in the FAR is evident, with high values distributed across the main island. Notably, the FAR values differ significantly between sites when comparing daily mean (from 0.33 to 1) and daily maximum (from 0.23 to 1) values, with high FAR being particularly noticeable in the Tokyo metropolitan area and part of the Sea of Japan side.

Figure 1c depicts the impact of human-induced change on the ensemble mean of daily mean SAT, calculated as HIST2022 minus NAT2022. The temperature increase is relatively large in the areas with high FAR and the distribution is similar to the FAR distribution. However, in fact, the increase is not necessarily large at high FAR sites because FAR is highly dependent on thresholds and shapes of probability distributions. Although the spatial distribution is similar in the GCM and RCM simulations, the high resolution of the RCM results in a stronger spatial contrast, which induces a twofold increase in the spatial standard deviation (SD), reflecting the complex terrain. Thus, human influence depends on the terrain, leading to regional variation in the temperature increase.

Modified atmospheric conditions

During the event, the Japanese 55-year Reanalysis (JRA-55; Kobayashi et al. 2015; Harada et al. 2016) displayed anticyclonic circulation with an intensity exceeding the 1.5-sigma level of internal annual variability over the main island (Fig. 2a). The center of the western North Pacific subtropical high (WNPSH) was shifted north of normal, which is often seen in the atmospheric response around Japan to a La Niña event (Iwakiri and Watanabe 2020). Although the intensity is weak, our simulations show a similar pattern.

The response of the sea level pressure (SLP) to human influence, estimated from HIST2022—NAT2022, shows a dipole pattern with positive and negative anomalies in the south and north of Japan, respectively, resulting in a change in the surface wind to a southwesterly over the main island (Fig. 2b, left). The NAT2022—NATc, which represents the SLP response to the 2022 SST pattern at the preindustrial level, exhibits a tripolar negative–positive–negative anomaly distribution from 20° to 45°N, caused by the northward shift of the WNPSH (Fig. 2b,

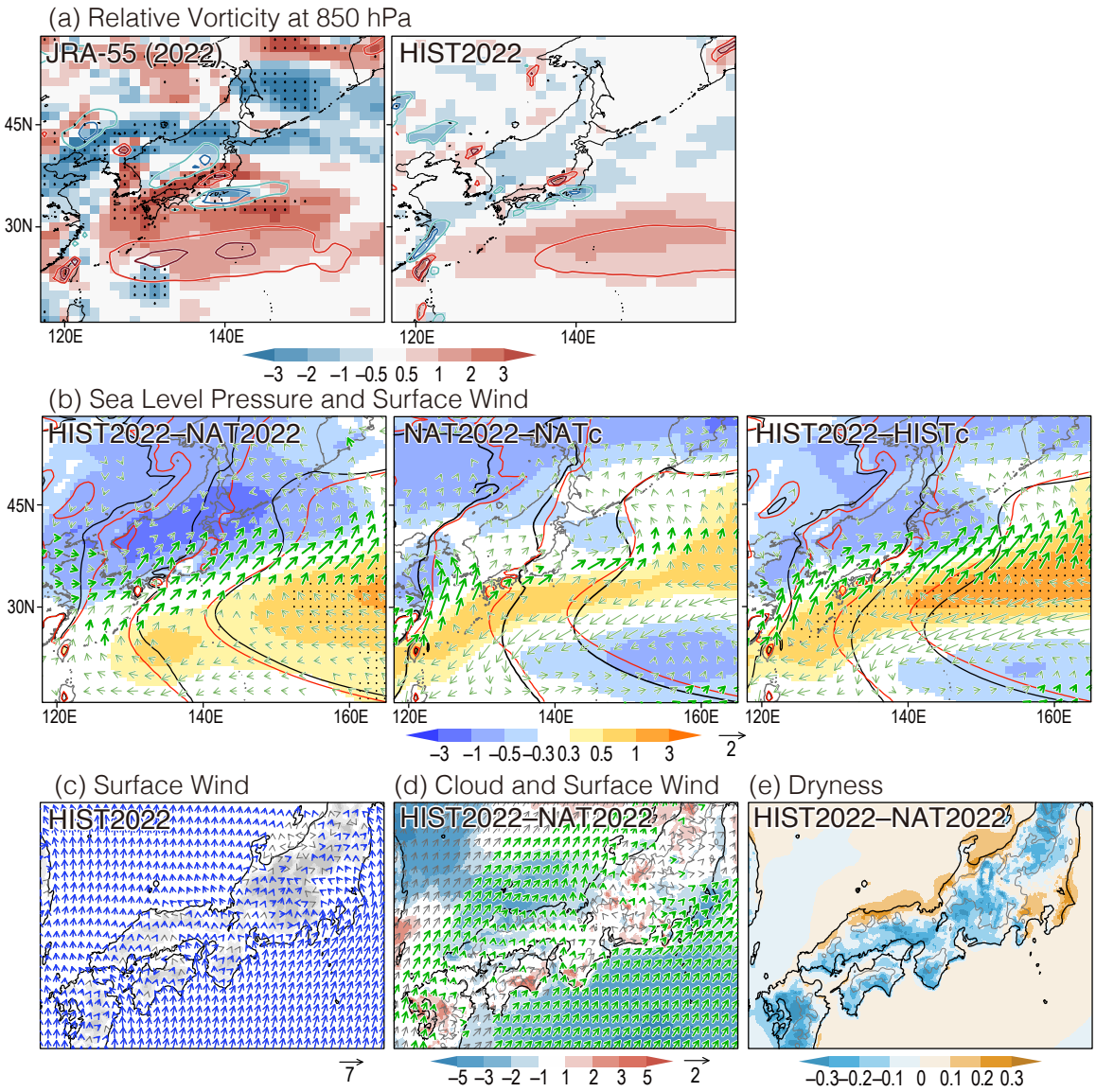

Fig. 2. (a) Relative vorticity at 850 hPa (s^{-1}) for (left) JRA-55 and (right) HIST2022 in the GCM. Contours indicate climatology at –1.5, –1, 1, and 1.5 s^{-1}. Stippled areas depict the 1.5-sigma level of the internal annual variability. (b) Differences in sea level pressure (shading) and surface wind (vectors) in the GCM for (left) HIST2022—NAT2022, (center) NAT2022—NATc, and (right) HIST2022—HISTc. Red and black contours indicate the pressures on minuend and subtrahend, respectively. Stippled areas indicate the difference is significant at the 95% confidence level. Vectors represent the wind difference over 0.2 m s^{-1}, with thick vectors showing a significant difference at the 95% level. (c) Surface wind in HIST2022. Blue vectors show wind exceeding 0.5 m s^{-1}. (d) Difference in cloud total amount (HIST2022—NAT2022; %). Vectors in (d) depict the difference in surface wind with thick vectors showing a significant difference at the 95% level. (e) Dryness at surface (HIST2022—NAT2022; K). The plots in (c)–(e) are the output from the 5-km RCM. Gray contours over land represent an altitude of 600 m.

middle). This SLP change promotes the southwesterly wind over western Japan. The positive and negative anomalies across Japan strengthen in HIST2022—HISTc (Fig. 2b, right). This is because HIST2022—HISTc represents the response to the 2022 SST pattern under global warming, corresponding to the impacts of NAT2022—NATc and HIST2022—NAT2022, as seen in the intensified upper two anomalies and, in contrast, the weakened negative anomaly at 20°N. The strengthening enhances the southwesterly over a larger area of the main island compared with NAT2022—NATc.

The wind change resulting from human influence, as indicated by HIST2022—NAT2022, significantly affects both the synoptic and regional scales, leading to modifications in regional circulation. Figure 2c depicts the surface wind simulated by the RCM. The areas on the Sea of Japan side that experience substantial temperature increases (Fig. 1c) are located mainly leeward of mountains, where the wind intensifies owing to the southwesterly change compared with NAT2022 (Fig. 2d). This intensified wind from the mountain areas significantly raises temperatures through terrain effects, such as the foehn phenomenon. Likewise, in the western parts of the Tokyo metropolitan area, a similar mechanism occurs around the mountain regions, whereas coastal areas are dominated by the flow from the sea (Fig. 2c). The southwesterly wind change disturbs the inland flow from the sea, resulting in decreased cloud cover (Fig. 2d) and increased dryness near the surface (SAT minus the dew temperature) (Fig. 2e), thereby altering the heat budget at the surface. As a result, noticeable temperature increases are observed in areas influenced by intensified terrain effects and the direct impacts of wind change caused by human-induced climate change, as seen in HIST2022—NAT2022.

Conclusions

This study utilized large-ensemble regional climate simulations with 5-km resolution to perform extreme event attribution for the 2022 high temperatures in Japan. The attribution of human-induced climate change to the high-temperature event varies across regions. The FAR index ranges from 0.33 to 1, with higher FAR being particularly noticeable in the Tokyo metropolitan area. During the event, a southwesterly wind change appeared over Japan as a response to natural variability, including the 2022 La Niña. Human-induced climate change intensified this wind change. The intensified southwesterly favored surface wind from the mountains in the mountain regions of the Tokyo metropolitan area while disrupting the wind from the sea in the coastal area. This resulted in noticeable temperature increases in these areas. These findings suggest that there are specific synoptic patterns associated with high temperatures in each region, and when human influence contributes to the formation of the pattern in a region, there is high attribution of human-induced change in that region.

Acknowledgments. This work was conducted under MEXT–Data Integration and Analysis System program (DIAS; JPMXD0721453504) and MEXT–program for the advanced studies of climate change projection (SENTAN; JPMXD0722680734 and JPMXD0722680395). All climate simulations were performed using the JAMSTEC Earth Simulator.

Data availability statement. The dataset of d4PDF and JRA-55 are publicly available from the DIAS at https://diasjp.net. The experimental data for the 2022 event can be provided upon request under the condition of collaborative research, within the limitations of the SENTAN program, MEXT, Japan.

References

Allen, M. R., 2003: Liability for climate change. *Nature*, **421**, 891–892, https://doi.org/10.1038/421891a.

Harada, Y., and Coauthors, 2016: The JRA-55 Reanalysis: Representation of atmospheric circulation and climate variability. *J. Meteor. Soc. Japan*, **94**, 269–302, https://doi.org/10.2151/jmsj.2016-015.

Hirahara, S., M. Ishii, and Y. Fukuda, 2014: Centennial-scale sea surface temperature analysis and its uncertainty. *J. Climate*, **27**, 57–75, https://doi.org/10.1175/JCLI-D-12-00837.1.

Imada, Y., S. Maeda, M. Watanabe, H. Shiogama, R. Mizuta, M. Ishii, and M. Kimoto, 2017: Recent enhanced seasonal temperature contrast in Japan from large ensemble high-resolution climate simulations. *Atmosphere*, **8**, 57, https://doi.org/10.3390/atmos8030057.

Imada, Y., M. Watanabe, H. Kawase, H. Shiogama, and M. Arai, 2019: The July 2018 high temperature event in Japan could not have happened without human-induced global warming. *SOLA*, **15A**, 8–12, https://doi.org/10.2151/sola.15A-002.

Inoue, M., A. Ugajin, O. Kiguchi, Y. Yamashita, M. Komine, and S. Yamakawa, 2021: Effects of the Tibetan high and the North Pacific high on the occurrence of hot or cool summers in Japan. *Atmosphere*, **12**, 307, https://doi.org/10.3390/atmos12030307.

Ito, R., H. Kawase, and Y. Imada, 2022: Regional differences in summertime extremely high temperature in Japan due to global warming. *J. Appl. Meteor. Climatol.*, **61**, 1573–1587, https://doi.org/10.1175/JAMC-D-22-0062.1.

Iwakiri, T., and M. Watanabe, 2020: Multiyear La Niña impact on summer temperature over Japan. *J. Meteor. Soc. Japan*, **98**, 1245–1260, https://doi.org/10.2151/jmsj.2020-064.

Kawase, H., and Coauthors, 2023: Identifying robust changes of extreme precipitation in Japan from large ensemble 5-km-grid regional experiments for 4K warming scenario. *J. Geophys. Res. Atmos.*, **128**, e2023JD038513, https://doi.org/10.1029/2023JD038513.

Kobayashi, S., and Coauthors, 2015: The JRA-55 Reanalysis: General specifications and basic characteristics. *J. Meteor. Soc. Japan*, **93**, 5–48, https://doi.org/10.2151/jmsj.2015-001.

Marshall, J., and F. Molteni, 1993: Toward a dynamical understanding of planetary-scale flow regimes. *J. Atmos. Sci.*, **50**, 1792–1818, https://doi.org/10.1175/1520-0469(1993)050<1792:TADUOP>2.0.CO;2.

Mizuta, R., and Coauthors, 2012: Climate simulations using MRI-AGCM3.2 with 20-km grid. *J. Meteor. Soc. Japan*, **90A**, 233–258, https://doi.org/10.2151/jmsj.2012-A12.

Mizuta, R., and Coauthors, 2017: Over 5,000 years of ensemble future climate simulations by 60-km global and 20-km regional atmospheric models. *Bull. Amer. Meteor. Soc.*, **98**, 1383–1398, https://doi.org/10.1175/BAMS-D-16-0099.1.

Piani, C., G. P. Weedon, M. Best, S. M. Gomes, P. Viterbo, S. Hagemann, and J. O. Haerter, 2010: Statistical bias correction of global simulated daily precipitation and temperature for the application of hydrological models. *J. Hydrol.*, **395**, 199–215, https://doi.org/10.1016/j.jhydrol.2010.10.024.

Sasaki, H., K. Kurihara, I. Takayabu, and T. Uchiyama, 2008: Preliminary experiments of reproducing the present climate using the non-hydrostatic regional climate model. *SOLA*, **4**, 25–28, https://doi.org/10.2151/sola.2008-007.

Shimpo, A., and Coauthors, 2019: Primary factors behind the heavy rain event of July 2018 and the subsequent heat wave in Japan. *SOLA*, **15A**, 13–18, https://doi.org/10.2151/sola.15A-003.

Takahashi, C., M. Watanabe, H. Shiogama, Y. Imada, and M. Mori, 2016: A persistent Japanese heat wave in early August 2015: Roles of natural variability and human-induced warming [in "Explaining Extreme Events of 2015 from a Climate Perspective"]. *Bull. Amer. Meteor. Soc.*, **97**, S107–S112, https://doi.org/10.1175/BAMS-D-16-0157.1.